Information Gap Decision Theory based OPF with HVDC Connected Wind Farms

Abbas Rabiee, *Member, IEEE,* Alireza Soroudi, *Member, IEEE,* Andrew Keane, *Senior Member, IEEE*

***Abstract*—A method for solving the optimal power flow (OPF) problem including HVDC connected offshore wind farms is presented in this paper. Different factors have been considered in the proposed method namely, voltage source converter (VSC-HVDC) and line-commutated converter high-voltage DC (LCC-HVDC) link constraints, doubly fed induction generators' (DFIGs) capability curve as well as the uncertainties of wind power generation. Information gap decision theory (IGDT) is utilized for handling the uncertainties associated with the volatility of wind power generation. It is computationally efficient and does not require the probability density function of wind speed. The proposed decision making framework finds the optimal decision variables in a way that they remain robust against the considered uncertainties. To illustrate the effectiveness of the proposed approach, it is applied on the IEEE 118-bus system. The obtained results validate the applicability of the proposed IGDT-based OPF model for optimal operation of AC/DC power systems with high penetration of offshore wind farms.**

***Index Terms*—HVDC, IGDT, OPF, uncertainty, wind power.**

NOMENCLATURE

Sets:

NB	Set of system buses
NG	Set of generators
NB_P	Set of buses connected to the pool market
NL	Set of transmission lines
$\Psi_{eq/ineq}$	Set of all equality/inequality constraints

Indecises:

b	Bus index
i	Generator index
m	Rectifier ($m = r$)/inverter ($m = i$)

AC network's variables and parameters:

P_{G_i}/Q_{G_i}	Active/reactive power generation by i^{th} thermal generation unit
P_{L_b}/Q_{L_b}	Active/reactive load in bus b
P_{wg}/Q_{wg}	Active/reactive power output of wind farm
Pp_b/Qp_b	Active/reactive power purchased from pool market
$P_{d,m}$	Active power flowing through HVDC link
φ_m	Angle difference between the fundamental line current and line-to-neutral AC voltage
P_w^{avl}	Actually available active power output of wind farm
P_w^{fr}	Forecasted active power output of wind farm
Y_{bj}/γ_{bj}	Magnitude/angle of bj^{th} element of Y_{bus}
$S_\ell(V,\theta)$	Power flow through ℓ^{th} transmission line.
Q_{wg}^{HV}	Reactive power output of wind farm received to the rectifier terminal of HVDC
$X_{tr,w}$	Reactance of step up transformer connecting offshore wind farm to HVDC (in pu)
$F_i(P_{G_i})$	The fuel cost function of i^{th} thermal generation unit
Pp_b/Qp_b	The purchased active/reactive power from the pool market at bus b.
V_b/θ_b	Voltage magnitude/angle in bus b

HVDC variables:

$R_{c,m}$	Commutation resistances
$V_{d,m}$	DC voltages at the HVDC terminals
I_d	DC current carried by the HVDC link
α_m	Ignition angle
$V_{d0,m}$	Ideal no-load voltage at the terminals
B_m	Number of series-connected bridges in a terminal
$R_{L,d}$	Resistance of HVDC cable
$Q_{d,m}$	Reactive power flowing into HVDC link
$B_{sh,m}$	Susceptance of HVDC shunt filters
T_m	Tap ratio of HVDC's transformer
$Q_{sh,m}$	VAR compensations at HVDC terminals
V_m	Voltage magnitudes of the AC terminals of HVDC
M_m	Amplitude modulation ratio in VSC-HVDC
Z_{T_m}	Impedance of HVDC coupling transformer

Risk associated variables:

$\Lambda_{c/o}$	Critical/opportunistic value of objective function to be maintained at presence of uncertainty
$\varsigma_{c/o}$	Critical/opportunistic percent of objective function used in risk averse/seeker strategy
$\hat{\zeta}, \check{\zeta}$	Maximum/minimum radius of uncertainty
Γ	Uncertainty set
γ	Uncertain parameter
ζ	Uncertain Radius of uncertainty

A. Rabiee is with the Department of Electrical Engineering, Faculty of Engineering, University of Zanjan, Zanjan 45371-38111, Iran, (e-mail: rabiee@znu.ac.ir).

Alireza Soroudi and Andrew Keane are with the School of Electrical, Electronic and Communications Engineering, University College Dublin, (e-mail: alireza.soroudi@ucd.ie, andrew.keane@ucd.ie) The work of A. Soroudi was conducted in the Electricity Research Centre, University College Dublin, Ireland, which is supported by the Commission for Energy Regulation, Bord Gáis Energy, Bord na Móna Energy, Cylon Controls, EirGrid, Electric Ireland, EPRI, ESB International, ESB Networks, Gaelectric, Intel, SSE Renewables, UTRC and Viridian Power & Energy. A. Soroudi is funded through Science Foundation Ireland (SFI) SEES Cluster under grant number SFI/09/SRC/E1780. A. Keane is supported by the SFI Charles Parsons Energy Research Awards SFI/06/CP/E005.

I. INTRODUCTION

A. Background and Motivation

UTILIZATION of wind power generation technology due to the economic and environmental concerns is taking substantial attention around the world. The aim of system operator (SO) is operating the system in a way that the total power generation cost is minimized for a given operating condition while satisfying the technical constraints and operational limits.

Such an optimization problem is called optimal power flow (OPF). The problem of uncertainty modelling of wind power generation is still an important issue [1]. Hence, the appropriate modelling of wind power generation in OPF formulation is essential.

In many countries, the optimal connection points for onshore wind farms are determined, and the utilities are willing to use offshore sites [2]. The offshore wind farm is located, generally, far away from the onshore grid. In case, the distance is long or if the offshore wind farm is connected to a weak AC onshore grid, a high-voltage dc (HVDC) transmission system would be preferred over the conventional high-voltage AC transmission [3].

B. Literature Review

The previous works which tackled the uncertainty modeling of wind power generation can be categorized as follows:

- Stochastic techniques
  - Monte Carlo Simulation [4], [5]
  - Point Estimate Method [6]
  - Scenario based modeling [7], [8]
- Fuzzy approach [9]
- Robust optimization [10]

Each technique has its own "pros and cons". For example, stochastic techniques require knowledge of the probability density function of uncertain parameter. It is usually computationally expensive and adds huge burden to the original problem. The fuzzy arithmetic requires a membership function for each uncertain parameter. It is usually difficult to deal with fuzzy numbers and they should be transformed into real valued numbers. The robust optimization requires knowledge of the range of variation of the uncertain parameters [11]. Additionally, it cannot be used in opportunistic cases to use possible positive impacts of uncertain parameters. It's not an easy task to choose the right uncertainty set for describing the uncertain parameters.

The gap which this work tries to fill is to propose a technique for handling the severe uncertainty associated with wind power generation. It is assumed that no range or probability density function or membership function is available.

Also, the previous researches for integration of uncertain wind farms using HVDC transmission, can be generally categorized based on the utilized technology and the main objectives of SO.

1) Utilized HVDC technology: Two types of HVDC transmission topologies, i.e., HVDC with voltage source converter (VSC-HVDC) using insulated gate bipolar transistors (IGBTs) and line-commutated converter HVDC (LCC-HVDC) are used today for offshore wind farm connectivity. Each technology has its own advantages and disadvantages, which are summarized as follows.

a) LCC-HVDC: The first commercial LCC-based HVDC link was commissioned in 1954 [12].

- Advantages: High reliability, little maintenance [13], suitable for offshore wind farm connection, high power capability [14], greater economies of scale, good overload capability, able to suppress DC side fault currents, lower converter losses and capital cost [15], well industrial experiences for connecting the offshore wind farms to the onshore AC network [16], robust to DC fault currents due to its current regulated nature [17].
- Disadvantages : Needs reactive power compensation in both AC terminals, possibility of commutation failures, large footprint, complicated coordination between active/reactive resources and HVDC station, minimum short circuit level restriction.

b) VSC-HVDC: The first commercial VSC-based HVDC link came in service in Sweden in 1997 [18].

- Advantages : Black start capability [19], no requirement for reactive power compensation, more compact and lighter compared to LCC, no need for harmonic filter, can be operated in both capacitive or inductive modes [20], [21], VSC valves are independent of the zero crossings of the current and balanced operation of the linked AC system, ability to control the negative sequence current injection in the offshore wind power plant [22], shorter design and installation times [15], using IGBT switches enables the VSC-HVDC scheme to be switched on and off at higher rate [23] and needs no external voltage source for commutation [24].
- Disadvantages : Lower reliability, weak overload capability, higher cost by 10-15% due to high component count, less mature technology, higher converters power losses due to witching operations (1.0- 1.5%), limited power capability, not able to suppress DC side fault currents [21].

Both of these HVDC technologies have their own cons and pros and choosing the best technology for HVDC link depends on the requirements of the planner, which is not the subject of this work. In this paper, both HVDC technologies are studied, but the main focus of the study will be on the LCC-HVDC transmission which is well utilized HVDC technology for connection of offshore wind farms to the onshore AC grids. This technology is the most established and widespread technology around the world [25].

2) The objective functions aimed by SO:

- Cost benefit analysis for the operational benefits against the investment costs of HVDC systems [26]
- Opportunity cost of wind power shortage & surplus [27]
- Cost of environmental benefit loss [27]
- Minimizing losses within the wind farm and the HVDC transmission system and maximizing production [28]
- Expected penalty cost for wind power curtailment [29]
- Expected cost of calling up power reserves because of wind power shortage [29]
- Risk due to expected energy not supplied (EENS) and total operating costs [30]
- Location marginal prices, and reserve costs [30]
- Voltage regulation of the electrical grid [31]

C. Contributions

In this paper, a new model is proposed for OPF problem of AC/DC power systems considering the uncertainty of wind power generation. The IGDT approach is employed to determine the best strategy for SO to procure the energy demand from

different resources. The LCC-HVDC transmission is utilized for connection the offshore wind farm to the AC onshore grid. Also, the objective function utilized in the proposed OPF model is minimization of total cost paid for energy procurement while making it robust against the undesired uncertainties or making more chance for receiving benefits from desired uncertainties. A number of works are reported in the literature to deal with the wind power uncertainties (e.g., [32]). However, to the best of authors' knowledge, no previous work in the literature deals with wind power uncertainty using IGDT approach specially when HVDC links are utilized. The contributions of this paper are three folds:

- Modelling the uncertainty of wind power generation without knowing the probability density function or membership function using information gap decision theory. The proposed model is tractable and does not add the complexity of the existing problem.
- The risk hedging technique is guarantees the decision makers objective function against the undesired effects of wind power volatility.
- The proposed model can be easily adopted by opportunistic decision makers in which they will seek positive benefits of uncertain wind power generation.

D. Paper Organization

The rest of this paper is organized as follows: Section II presents problem formulation, the proposed information gap decision theory (IGDT) technique is presented in Section III. Simulation results are presented in Section IV and finally, Section V summarizes the findings of this work.

II. OPF Problem Formulation

The AC/DC power flow equations, HVDC link model and characteristics of DFIG-based wind farms are formulated in this section. The assumptions, objectives, decision variables and constraints are described in this section. The decision variables of the problem include: Generation schedule and terminal voltage of thermal units, Var injections at both terminals along with the tap settings of on-load tap changers of HVDC links. The proposed robust decision making framework finds the optimal values for these variables considering the uncertainty of wind power generation outputs.

A. Load Flow Equations of AC Network

The load flow equations of the AC side of the system ($\forall b \in NB$) are:

$$P_b^{net} = \sum_{j=1}^{NB} V_b V_j Y_{bj} cos(\theta_b - \theta_j - \delta_{bj}) \quad (1)$$

$$P_b^{net} = \sum_{i=1}^{NG} P_{G_i} + Pp_b - P_{L_b} \quad (2)$$

$$Q_b^{net} = \sum_{j=1}^{NB} V_b V_j Y_{bj} sin(\theta_b - \theta_j - \delta_{bj}) \quad (3)$$

$$Q_b^{net} = \sum_{i=1}^{NG} Q_{G_i} + Qp_b - Q_{L_b} \quad (4)$$

and the following limits are considered.

$$P_{G_i}^{min} \le P_{G_i} \le P_{G_i}^{max} \quad \forall i \in NG \quad (5)$$

$$Q_{G_i}^{min} \le Q_{G_i} \le Q_{G_i}^{max} \quad \forall i \in NG \quad (6)$$

$$V_b^{min} \le V_b \le V_b^{max} \quad \forall b \in NB \quad (7)$$

$$|S_\ell(V,\theta)| \le S_\ell^{max} \quad \forall \ell \in NL \quad (8)$$

$$Pp_b^{min} \le Pp_b \le Pp_b^{max} \quad \forall b \in NB_P \quad (9)$$

$$Qp_b^{min} \le Qp_b \le Qp_b^{max} \quad \forall b \in NB_P \quad (10)$$

B. LCC-HVDC OPF Model

In LCC-HVDC technology which uses thyristor valves, the valves can only switch off when their current becomes zero. The proper commutation depends on the normal and balance operation of the connected AC network. The delayed ignition of the thyristors leads to the lagged AC current flowing to the converters, respect to the AC voltage of the terminal. Thus, reactive power is absorbed by a LCC-HVDC link in its AC side of both rectifier and inverter terminals. The schematic of LCC-HVDC link is depicted in Fig. 1. Load flow equations of the LCC-HVDC system is as follows. The steady state model of this system which is suitable for OPF model, is given in the following. For $m = r, i$ (r: Rectifier, i: Inverter):

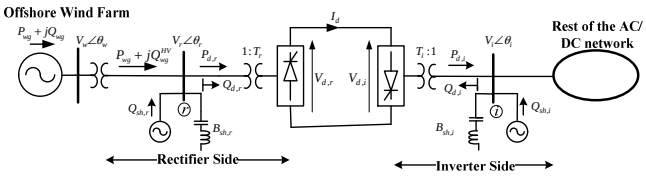

Fig. 1. Single-line diagram of wind farm connected via LCC-HVDC transmission link

$$V_{d0,m} = \frac{3\sqrt{2}}{\pi} B_m T_m V_m \quad (11)$$

$$V_{d,m} = V_{d0,m} cos(\alpha_m) - B_m R_{c,m} I_d \quad (12)$$

$$I_d = \frac{V_{d,r} - V_{d,i}}{R_{L,d}} \quad (13)$$

$$cos(\varphi_m) = \frac{V_{d,m}}{V_{d0,m}} \quad (14)$$

$$P_{d,m} = V_{d,m} I_d \quad (15)$$

$$Q_{d,m} = P_{d,m} tan(\varphi_m) \quad (16)$$

where (11) gives the relationship between ideal no-load voltage at the DC sides of the LCC-HVDC link, and the AC sides voltages. Equation (12) is the actual voltages at both DC terminals due to the commutation overlap, and (13) is the DC current flowing through HVDC. Also, (14) is the power factors at the HV buses of HVDC link's AC sides. Constraints (15), (16) are the DC active powers (which are equal to AC active powers), and the reactive power absorbed by the HVDC link's AC terminals By neglecting the converters' losses, respectively.

It is worth to note that, $Q_{d,i}$ and $Q_{d,r}$ are reactive power, flowing into AC sides of the HVDC link. In other words, $Q_{d,i}$ and $Q_{d,r}$ are the reactive power absorption by the HVDC in the AC terminals of inverter and rectifier sides, respectively. These reactive power absorptions are necessary for proper commutation of LCC converters. Also, the following limits are considered in the proposed OPF model:

$$0 \leq P_{d,m} \leq P_d^{max} \tag{17}$$
$$V_{d,m}^{min} \leq V_{d,m} \leq V_{d,m}^{max} \tag{18}$$
$$Q_{d,m}^{min} \leq Q_{d,m} \leq Q_{d,m}^{max} \tag{19}$$
$$Q_{sh,m}^{min} \leq Q_{sh,m} \leq Q_{sh,m}^{max} \tag{20}$$

C. DFIG-based wind farm steady state model

Doubly fed induction generator (DFIG) is a three-phase wound-rotor induction machine. The mechanical power at the machine shaft is converted into electrical power supplied to the ac power network via both the stator and rotor windings. The machine operates like a synchronous generator whose synchronous speed (i.e., the speed at which the generator shaft must rotate to generate power at the ac power network frequency) can be varied by adjusting the frequency of the ac currents fed into the rotor windings. One salient feature of DFIG is the capability of reactive power exchange between the generator and the AC power network which is constrained by a capability curve that determines the feasible operating region in the PQ plane.

In order to study the steady state behavior of DFIG-based wind farms properly, it is necessary to model the DFIG's active/reactive power capability curve [33]. In this paper it is modelled based on the assumptions and considerations given in [33], [34]. The following limits are considered:

1) Stator/rotor current limit
2) Steady state stability limit
3) Total Capability limit
4) Wind-Turbine maximum/minimum active power output limit

Hence, active and reactive power production limits of DFIG-based wind farm are as follows.

$$0 \leq P_{wg} \leq P_{wg}^{avl} \tag{21}$$
$$Q_{wg}^{min} \leq Q_{wg} \leq Q_{wg}^{max} \tag{22}$$

D. Load Flow Equations at the Interface of AC/DC Networks for LCC-HVDC

According to Fig. 1, at the inverter side of the HVDC connection (i.e. bus i), the power balance equations of joint AC/DC networks are as follows.

$$P_i^{net} = P_{G_i} + P_{d,i} - P_{L_i} \tag{23}$$
$$Q_i^{net} = Q_{G_i} + B_{sh,i}V_i^2 + Q_{sh,i} - Q_{d,i} - Q_{L_i} \tag{24}$$

From Fig. 1, at the rectifier side by neglecting active power losses of the transformers connecting the wind farm to the HVDC rectifier terminal, the power balance equations of AC/DC networks are as follows.

$$P_{d,r} = P_{wg} \tag{25}$$
$$Q_{d,r} = Q_{wg}^{HV} + B_{sh,r}V_r^2 + Q_{sh,r} \tag{26}$$
$$Q_{wg}^{HV} = \frac{V_r}{X_{tr,w}}(V_w cos(\theta_w - \theta_r) - V_r) \tag{27}$$
$$Q_{wg} = \frac{V_w}{X_{tr,w}}(V_w - V_r cos(\theta_w - \theta_r)) \tag{28}$$

E. VSC-HVDC OPF Model

The single line diagram of VSC-HVDC is depicted in Fig. 2. For the purpose of fundamental frequency analysis each converter station is represented by a complex voltage source $E_m \angle \sigma_m$ behind its transformer impedance Z_{T_m} ($\forall m = r, i$). In other words, two AC buses are added to the system, representing the AC sides of the VSC. Thus, equivalently, two buses are added to the system in the conventional OPF model. The equivalent circuit of VSC-HVDC is depicted in Fig. 3. In contrary to the case of LCC-HVDC, not only the VSC technology does not need reactive power compensation in the AC side terminals, but also it can control both active and reactive power flows independently in AC sides, which is a great advantage. Hence in the case of VSC-HVDC, both $B_{sh,m}$ and $Q_{sh,m}$ are zero in the interface of AC/DC systems. Also, the equation (29) is introduced which reflects the relation between the DC voltage across the capacitor bank in the DC sides, and the corresponding converted AC voltage at the rectifier and inverter sides [35], [36].

$$E_m = \frac{M_m}{2\sqrt{2}}V_{d,m} \tag{29}$$
$$I_d = \frac{V_{d,r} - V_{d,i}}{R_{L,d}} \tag{30}$$
$$P_{d,m} = V_{d,m}I_d \tag{31}$$

where, M_m is amplitude modulation ratio [36], and $0 \leq M_m \leq 1$ [35]. Besides, the limits on the active/reactive power flow of converters are the same with the LCC case, which is given by equations (17)-(19).

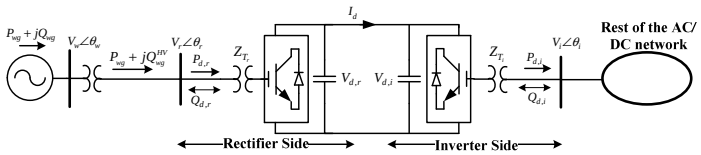

Fig. 2. Single-line diagram of wind farm connected via VSC-HVDC transmission link

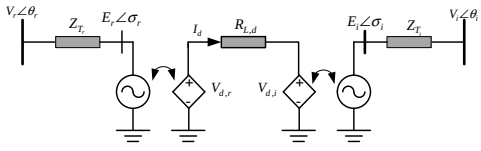

Fig. 3. Equivalent circuit of the VSC-HVDC transmission link

F. Load Flow Equations at the Interface of AC/DC Networks for VSC-HVDC

Similar to the LCC-HVDC, according to Fig. 2 at the inverter side OF VSC-HVDC (i.e. bus i) the power balance equations of AC/DC systems are as follows.

$$P_i^{net} = P_{G_i} + P_{d,i} - P_{L_i} \tag{32}$$
$$Q_i^{net} = Q_{G_i} - Q_{d,i} - Q_{L_i} \tag{33}$$

Also, at the rectifier side, the power flow equations of mixed AC/DC networks are as follows.

$$P_{d,r} = P_{wg} \tag{34}$$
$$Q_{d,r} = Q_{wg}^{HV} \tag{35}$$

where Q_{wg}^{HV} is obtained from (27).

G. Objective function

The objective function of the IGDT based OPF problem to be minimized is defined as the total cost paid for energy balance and is calculated as follows:

$$\min_{DV} TC = \sum_{b}(Pp_b\lambda_b) + \sum_{i} F_i(P_{G_i}) \tag{36}$$

where $F_i(P_{G_i})$ is the fuel cost function (in $\$/h$), which is modelled by a quadratic function as follows.

$$F_i(P_{G_i}) = a_i P_{G_i}^2 + b_i P_{G_i} + c_i \tag{37}$$

III. IGDT based Uncertainty Modelling of Wind Power Generation

In this paper, an IGDT based model [37] is proposed to handle the uncertainty of wind power generation. The proposed method does not need any probability density function. It is exact and computationally efficient. Without loss of generality, the minimization procedure is explained and discussed in this section. The general optimization problem is expressed as follows:

$$\min_{X} f(X,\gamma) \tag{38}$$
$$\mathbf{H}_i(X,\gamma) \leq 0, i \in \Psi_{eq} \tag{39}$$
$$\mathbf{G}_j(X,\gamma) = 0, j \in \Psi_{ineq} \tag{40}$$
$$\gamma \in \Gamma \tag{41}$$

γ is the vector of input uncertain parameters. Γ is the uncertainty set describing the behavior of uncertain input parameters. X is the set of decision variables. The uncertainty set can be mathematically described as follows:

$$\forall\gamma \in \Gamma(\bar{\gamma},\zeta) = \left\{\gamma : \left|\frac{\gamma-\bar{\gamma}}{\bar{\gamma}}\right| \leq \zeta\right\} \tag{42}$$

$\bar{\gamma}$ is the forecasted value of the uncertain parameter. ζ is the maximum possible deviation of actual realization of uncertain parameter from its predicted value. It is also called "the radius of uncertainty" which itself is uncertain for the decision maker. One trivial strategy to deal with (38) to (41) is assuming that the uncertain parameter would not deviate from its predicted value as follows:

$$f_b = \min_{X} f(X,\bar{\gamma}) \tag{43a}$$
$$\mathbf{H}_i(X,\bar{\gamma}) \leq 0, i \in \Psi_{eq} \tag{43b}$$
$$\mathbf{G}_j(X,\bar{\gamma}) = 0, j \in \Psi_{ineq} \tag{43c}$$

Let's call the outcome of (43) the basic value of objective function (f_b). The question which may rise here is that what will happen if the realized uncertain parameter is different with what is predicted. Two different strategies may be adopted by the decision maker to face with the mentioned uncertainty.

- Risk averse: Is it possible to set the decision variables in order to avoid undesired impacts of uncertainties?
- Risk seeker: Is it possible to set the decision variables in order to make some benefits of possible uncertainties?

A. Risk averse strategy

This strategy tries to make the obtained (f_b) robust against the possible errors in predicting the uncertain input parameters. This strategy is usually chosen by conservative decision makers. The decision variable set should be optimally found in a way that the actual objective function f remain immune (to some degree) against the deviation of uncertain parameter γ from its predicted value $\bar{\gamma}$. It is obvious that the most robust decision is reached when the objective function is immunized against the maximum radius of uncertainty (ζ). This is mathematically formulated as follows:

$$\max_{X} \hat{\zeta} \tag{44a}$$
$$\mathbf{H}_i(X,\gamma) \leq 0, i \in \Psi_{eq} \tag{44b}$$
$$\mathbf{G}_j(X,\gamma) = 0, j \in \Psi_{ineq} \tag{44c}$$
$$\left\{\begin{array}{c} \hat{\zeta} = \max_{\zeta} \zeta \\ f(X,\gamma) \leq \Lambda_c \\ \Lambda_c = f_b(X,\gamma) + \varsigma_c \left|f_b(X,\gamma)\right|, \gamma \in \Gamma \end{array}\right\} \tag{44d}$$

Λ_c is the critical value that the objective function should be immunized against surpassing it. It can be defined based on the requirements of the decision maker. However it is usually defined as a function of the base objective function. In this work, ς_c is used to define the Λ_c. ς_c is a positive parameter set by the decision maker. It specifies the degree of acceptable tolerance on increasing (deteriorating) the value of base objective function (f_b) due to the possible undesired uncertainties. The formulation described in (44) has a bi-level structure. In the lower level (44d), the maximum radius of uncertainty ($\hat{\zeta}$) for a given value of X is determined. Then this radius of uncertainty will be passed to the upper level (i.e. (44a)-(44c)). In the upper level, decision maker sets the decision variable X to increase the $\hat{\zeta}$ (increase the immunity). In this way, the success (not increasing the objective function more than (f_b) with specified tolerance level) is achievable even when large deviation of uncertain parameters from their predicted values occurs.

Thus, the above risk averse strategy is customized for the proposed OPF model, as follows.

$$TC_b = \min_{DV}\left\{\sum_{b}(Pp_b\lambda_b) + \sum_{i} F_i(P_{G_i})\right\}_{P_{wg}^{avl}=P_{wg}^{f}} \tag{45a}$$
$$(1)to(37) \tag{45b}$$

TC_b is the total cost for the base case (where there is no forecast error). The next step is adding two more constraints to (45) as follows:

$$\max_{DV\cup\zeta} \zeta \tag{46a}$$
$$(1)to(37) \tag{46b}$$
$$TC \leq TC_b + |TC_b|\,\varsigma_c \tag{46c}$$
$$P_{wg}^{avl} = P_{wg}^{f}(1-\zeta) \tag{46d}$$

In other words, the immunity (TC remains below a reasonable limit) is sought when wind power generation is less than what it was expected to be (due to lower wind speed in the site, non-optimal power tracking function and etc).

B. Risk seeker strategy

This strategy tries to make the obtained (f_b) robust against the possible errors in prediction of the uncertain input parameters. This strategy is usually chosen by optimistic decision makers. In contrary to the risk averse strategy explained in section III-A, the decision maker is optimistically looking at the possible uncertain events that may positively affects the objective function (further reduces it). In risk seeker approach, the decision variables are set in a way that this can happen even with slight error (minimum radius of uncertainty) in prediction of uncertain parameters. This is mathematically formulated as follows:

$$\min_{X} \check{\zeta} \tag{47a}$$
$$\mathbf{H}_i(X,\gamma) \leq 0, i \in \Psi_{eq} \tag{47b}$$
$$\mathbf{G}_j(X,\gamma) = 0, j \in \Psi_{ineq} \tag{47c}$$
$$\left\{ \begin{array}{c} \check{\zeta} = \min_{\zeta} \zeta \\ f(X,\gamma) \leq \Lambda_o \\ \Lambda_o = f_b(X,\gamma) - \varsigma_o \left| f_b(X,\gamma) \right|, \gamma \in \Gamma \end{array} \right\} \tag{47d}$$

Λ_o is the opportunity value that the objective function should be less than it (in minimization approach). It is defined based on the greediness of the decision maker. However it is usually defined as a function of the base objective function. In this work, ς_o is used to defined the Λ_o. ς_o is a positive parameter set by the decision maker. It specifies the degree of greediness on further decreasing (improving) the value of base objective function (f_b) due to the possible uncertainties. The formulation described in (47) has a bi-level structure. In the lower level (47d), the maximum radius of uncertainty ($\check{\zeta}$) for a given value of X is determined. Then this radius of uncertainty will be passed to the upper level (47a) to (47c). In the upper level, decision maker sets the decision variable X to decrease the $\check{\zeta}$. In this way, the success (decreasing the objective function even more than (f_b)) is achievable even when small deviation of uncertain parameters from their predicted values happens. In the proposed OPF model, similar to section III-A, TC_b is found using (45). The next step is adding two more constraints to (45) as follows:

$$\min_{DV \cup \zeta} \check{\zeta} \tag{48a}$$
$$(1) to (37) \tag{48b}$$
$$TC \leq TC_b - |TC_b| \varsigma_o \tag{48c}$$
$$P_{wg}^{avl} = P_{wg}^{f}(1+\zeta) \tag{48d}$$

IV. Simulation results

A. Data

The proposed OPF model is examined on the IEEE 118-bus system. This system consists of 54 generator buses, and 186 transmission lines. The data of this system including the data of loads, generating units and transmission lines are given in [38]. The load level given in [38] is 20% higher than the original value for this system, given in [39]. The proposed algorithm is implemented in GAMS [40] environment solved by SNOPT solver running on an Intel®Xeon™CPU E5-1620 3.6 GHz PC with 8 GB RAM. In this study, two wind farms (WFs) are considered and the capacity of each farm is 1000 MW. WF-1 and WF-2 are connected to buses B_{25} and B_{90}, respectively. It is worth to mention that these buses are selected arbitrary. It is assumed that the energy resources (or energy procurement options) are the mentioned wind farms, thermal units and also the pool market. The purchased power from pool market is injected to the network through slack bus which is bus B_{69}. Besides, the cost of energy procurement from pool market is assumed to be \$40/MWh.

B. Analysis in the presence of LCC-HVDC

In this case, it is assumed that each WF is connected to the system via a 24-pulse LCC-HVDC link. HVDC links are bipolar with the rating of 1000 MW, 250 kV. The data of these DC links derived from [41]. Three case studies are analyzed in this work as follows:

- Base case (BC): In this case, it is assumed that all uncertain parameters (wind power generation) will be equal to their forecasted values.
- Risk averse (RA): In this case, the decision variables (U) are optimally found in order to increase the robustness of the objective function.
- Risk seeker (RS): In this case, the decision variables (U) are optimally found in order to increase the chance of further decrease in objective function.

1) Base case (BC): As it was already explained, the first step in IGDT analysis is calculating the base case for objective function. It is assumed that the forecasted wind power generation is 80% of its installed capacity for both wind farms. The total cost of energy procurement including thermal unit generation and pool market costs is equal to TC_b=\$167072.7308. The active and reactive power purchased from pool market in BC are Pp_b=79.6247 MW, Qp_b=274.5901 MVAR ($\forall b = B_{69}$), respectively. Also, the optimal schedule of wind farms' active/reactive power outputs, along with the required reactive power compensation at the HVDC terminals are given in Table I. Besides, the optimal active power schedule of thermal generation units, in BC are given in Table II, and the corresponding voltage values at the generator buses in BC are depicted in Fig. 4 (in green). Table III gives the optimal values of HVDC variables for BC.

In this case, total active power demand and total active power losses of the system are 5090.4000 MW and 222.6381 MW, respectively. Thus, the percent of participation of different energy procurement options to supply the sum of system load and losses (i.e. 5313.0381 MW) in this case are 68.39% for thermal generation units, 30.11% for wind farms and 1.5% for pool market.

TABLE I
THE OPTIMAL SCHEDULE OF WIND FARMS IN BC STRATEGY (LCC-HVDC)

WF No.	$P_{wg}(MW)$	$Q_{wg}(MVAR)$	$Q_{sh,r}(MVAR)$	$Q_{sh,i}(MVAR)$
WF-1	800	-67.8231	500	321.0941
WF-2	800	-96.3061	500	-38.8547

TABLE II
THE OPTIMAL ACTIVE POWER SCHEDULE OF THERMAL UNITS IN DIFFERENT CASES (IN MW) FOR LCC-HVDC

Bus No.	BC	RA	RS	Bus No.	BC	RA	RS
B_1	71.76	73.11	70.02	B_{65}	211.32	214.85	206.75
B_4	29.36	37.30	19.23	B_{66}	75.00	75.00	75.00
B_6	18.51	22.10	13.89	B_{69}	141.59	141.59	141.59
B_8	80.55	84.20	75.69	B_{70}	10.00	10.00	10.00
B_{10}	78.25	82.79	72.19	B_{72}	10.00	10.00	10.00
B_{12}	165.32	168.74	160.65	B_{73}	31.96	37.01	22.16
B_{15}	33.07	44.49	16.25	B_{74}	100.00	100.00	100.00
B_{18}	10.00	10.00	10.00	B_{76}	100.00	100.00	100.00
B_{19}	100.00	100.00	100.00	B_{77}	10.00	30.71	10.00
B_{24}	10.00	20.26	10.00	B_{80}	208.84	222.98	190.79
B_{25}	40.00	40.00	40.00	B_{85}	10.00	10.00	10.00
B_{26}	45.00	45.00	45.00	B_{87}	12.00	12.00	12.00
B_{27}	10.00	21.04	10.00	B_{89}	100.00	100.00	100.00
B_{31}	31.95	45.61	10.00	B_{90}	10.00	10.00	10.00
B_{32}	10.00	15.11	10.00	B_{91}	10.00	10.00	10.00
B_{34}	60.55	69.33	49.25	B_{92}	10.00	10.00	10.00
B_{36}	61.42	65.86	55.70	B_{99}	95.14	100.00	81.43
B_{40}	100.00	100.00	100.00	B_{100}	25.00	25.00	25.00
B_{42}	100.00	100.00	100.00	B_{103}	28.72	48.78	15.00
B_{46}	119.00	119.00	119.00	B_{104}	10.00	10.00	10.00
B_{49}	35.00	35.00	35.00	B_{105}	84.62	93.48	75.23
B_{54}	148.00	148.00	148.00	B_{107}	52.80	57.92	47.42
B_{55}	100.00	100.00	100.00	B_{110}	23.62	27.39	19.12
B_{56}	100.00	100.00	100.00	B_{111}	27.12	28.14	26.07
B_{59}	223.02	224.53	221.06	B_{112}	91.45	92.33	90.46
B_{61}	237.14	240.80	232.37	B_{113}	14.31	24.57	10.00
B_{62}	12.00	12.00	12.00	B_{116}	100.00	100.00	100.00

TABLE III
THE OPTIMAL SETTINGS OF LCC-HVDC LINKS IN DIFFERENT CASES

Variable	BC		RA		RS	
	$HVDC_1$	$HVDC_2$	$HVDC_1$	$HVDC_2$	$HVDC_1$	$HVDC_2$
$\phi_r(Rad)$	0.3933	0.3618	0.3934	0.3618	0.3925	0.3845
$\phi_i(Rad)$	0.3683	0.4017	0.3424	0.3782	0.4312	0.3959
$\alpha_r(Rad)$	0.1886	0.1037	0.2369	0.1773	0.1136	0.0800
$\alpha_i(Rad)$	0.0953	0.1895	0.1129	0.1988	0.1929	0.0800
$V_{d,r}(kV)$	550.0000	550.0000	550.0000	550.0000	550.0000	550.0000
$V_{d,i}(kV)$	520.9091	520.9091	525.9558	525.9558	515.4834	515.4834
$V_{d0,r}(kV)$	595.4689	588.0700	595.4800	588.0700	595.2569	593.3175
$V_{d0,i}(kV)$	558.3538	565.9496	558.3611	565.9508	567.4247	558.6902
$P_{d,r}(MW)$	800.0000	800.0000	661.2148	661.2148	949.2064	949.2064
$P_{d,i}(MW)$	757.6860	757.6860	632.3087	632.3087	889.6366	889.6366
$Q_{d,r}(MVAR)$	331.9532	302.7632	274.3999	250.2394	392.9088	384.0725
$Q_{d,i}(MVAR)$	292.4063	321.8217	225.3544	251.2322	409.3081	371.8015
$T_r(pu)$	0.4727	0.4668	0.4727	0.4668	0.4725	0.4710
$T_i(pu)$	0.4432	0.4493	0.4432	0.4493	0.4504	0.4435
$I_d(kA)$	1.4545	1.4545	1.2022	1.2022	1.7258	1.7258
$V_r(kV)$	233.2000	233.2000	233.2000	233.2000	233.2000	233.2000
$V_i(kV)$	233.2000	233.2000	233.2000	233.2000	233.2000	233.2000

2) Risk averse (RA) strategy: In this case, variation of participation from different procurement options versus conservativeness parameter ς_c are illustrated in Fig. 5. Also, Fig. 6 shows the ratio of different energy procurement options to their corresponding base case values, when parameter ς_c varies from zero to its maximum value of 0.35. It is observed from these figure that by increasing ς_c, the participation of wind farms in energy procurement decreases, whereas in contrary, the participation of thermal generation units and pool market are increased, which shows more conservative decisions for larger values of ς_c. Also, Fig. 7 and Fig. 8 show the variation of active/reactive power outputs of wind farms and reactive power compensation at the HVDC terminals, vs ς_c. It is observed from Fig. 7 that, by increasing the conservativeness factor, ς_c, the active power output of wind farms decreases, which leads to more absorption of reactive power by wind farms. Also, it is observed from Fig. 8 that, by increasing the ς_c, reactive power injections by the VAR compensator located at the rectifier sides remain constant for $\varsigma_c < 0.20$, but, beyond this value and for $0.20 \leq \varsigma_c < 0.30$, they begin to decrease, which is due to the fact that the VAR absorption by DFIGs in wind farms reaches to its lower limit for both wind farms. For $\varsigma_c > 0.30$, both reactive power absorptions and injections at the rectifier sides diminish, and finally become zero for $\varsigma_c = 0.35$, because, the generated power by wind farms and consequently transmitted power through HVDC links become zero. Also, it is observed from Fig. 8 that the reactive power injections at the inverter (or network side) of the HVDC, monotonically decrease as a result of reduction in active power transmission via HVDC link.

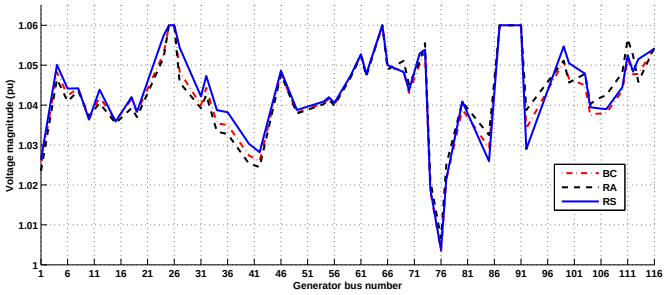

Fig. 4. Voltage at generator nodes (pu) in different cases for LCC-HVDC ($\varsigma_c = \varsigma_o = 5\%$)

Among the aforementioned different values of ς_c (i.e. acceptable tolerance in deterioration of TC), the optimal values of decision variables are given for $\varsigma_c = 5\%$, in RA case. For the above acceptable tolerance, the total energy procurement cost is equal to TC_b=\$167072.7308$\times$(1+0.05)= \$175426.3674. Also in this case, for $\varsigma_c = 5\%$ the percent of participation of different energy procurement options are 72.94% for thermal generation units, 25.21% for wind farms and 1.85% for pool market. Besides, it is observed form Fig. 6 that in RA strategy wind power participation reduces 16.26%, while thermal power generation and the power import from pool market increase 6.66% and 23.49%, respectively.

The optimal active power schedule of thermal generation units in this case for $\varsigma_c = 5\%$, are given in Table II. Also, the optimal voltage settings of generator buses are depicted in Fig. 4 (in black). The active and reactive power purchased from pool market in RA strategy are Pp_b=96.9809 MW, Qp_b=277.9948 MVAR ($\forall b = B_{69}$), respectively. Besides, the optimal active/reactive power outputs of wind farms and the corresponding reactive power compensation at both rectifier and inverter sides of HVDC links are given in Table IV. Also, the optimal values of HVDC variables for RA strategy are given in Table III.

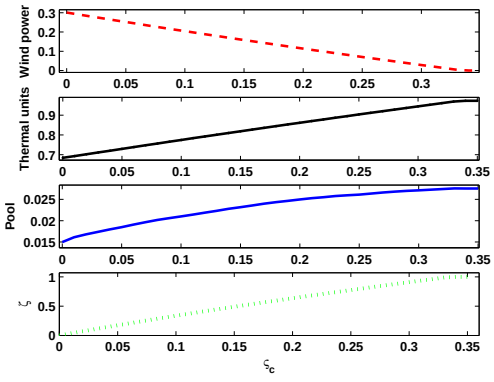

Fig. 5. Participation from different procurement options in RA strategy (LCC-HVDC)

3) Risk seeker (RS) strategy: In this case, variation of participation from different procurement options versus opportuneness parameter ς_o are illustrated in Fig. 9. It is observed from this figure that by increasing ς_o, the participation of wind farms

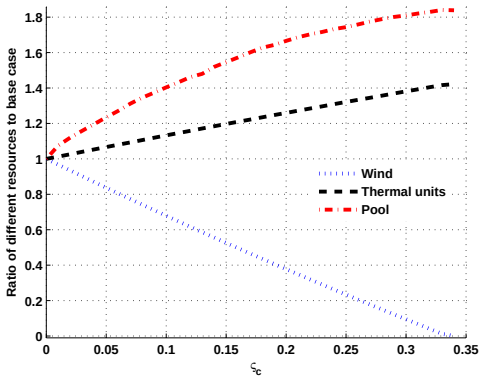

Fig. 6. Ratio of different resources to their corresponding base case values vs ς_c in RA strategy (LCC-HVDC)

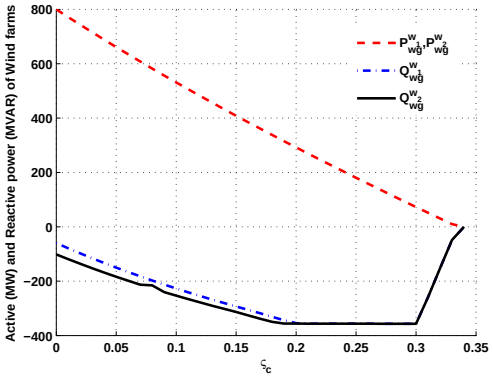

Fig. 7. Variations of active and reactive power of wind farms vs ς_c in RA strategy (LCC-HVDC)

in energy procurement increase, while contrarily, the share of thermal generation units and pool market decreases, which results in decisions with higher risk level for larger values of ς_o. Also, Fig. 10 gives the ratio of different energy procurement options to their corresponding base case values, when parameter ς_o increases from zero to its maximum permissible value of 0.065. Also, variation of active and reactive power outputs of wind farms are depicted in Fig. 11, whereas the VAR injections through VAR compensator at rectifier and inverter sides are shown in Fig. 12. It is observed from these two figures that by increasing the ς_o, active and power generation by wind farms increase, thus the active power transmitted via HVDC links are also increase, correspondingly. Consequently, the VAR injections by reactive power compensator at inverter side are increases. It is worth to note that, in this mode of operation, VAR outputs of compensator at rectifier sides remains constant at their maximum value of 500 MVAR, due to the increasing level of active power delivery through HVDC links. Similar to RA strategy, the optimal schedule of different variables are given for the opportuneness degree, $\varsigma_o = 5\%$. Active and reactive power purchased from pool market for $\varsigma_o = 5\%$ is Pp_b=49.4333 MW, Qp_b=274.6714 MVaR, respectively. Also, active power schedule of thermal generation units are given in Table II. The optimal voltage levels in generator buses are also depicted in Fig. 4 (in red). Also, the optimal values of HVDC links' variables are given in Table III. Finally, Table V summarizes the active/reactive power generation by wind farms,

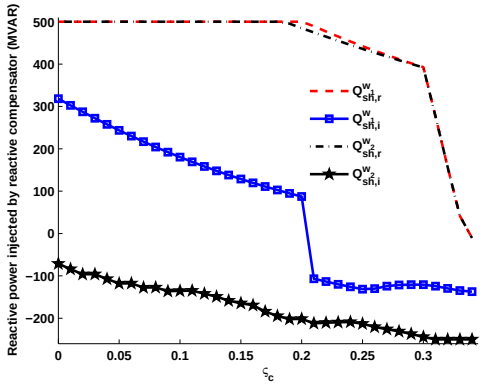

Fig. 8. Variation of reactive power injections vs ς_c at both sides of HVDC links in RA strategy (LCC-HVDC)

TABLE IV
THE OPTIMAL SCHEDULE OF WIND FARMS IN RA STRATEGY (LCC-HVDC)

WF No.	$P_{wg}(MW)$	$Q_{wg}(MVAR)$	$Q_{sh,r}(MVAR)$	$Q_{sh,i}(MVAR)$
WF-1	661.2148	-156.6384	500	246.1451
WF-2	661.2148	-179.5614	500	-100.3445

and their corresponding VAR compensations for $\varsigma_o = 5\%$.

TABLE V
THE OPTIMAL SCHEDULE OF WIND FARMS IN RS STRATEGY (LCC-HVDC)

WF No.	$P_{wg}(MW)$	$Q_{wg}(MVAR)$	$Q_{sh,r}(MVAR)$	$Q_{sh,i}(MVAR)$
WF-1	949.2064	35.9547	500	437.9988
WF-2	949.2064	26.8379	500	7.7617

C. Analysis in the presence of VSC-HVDC

In this case, VSC-HVDC technology is utilized for connection of the offshore WFs to the onshore gird. It is assumed that the DC cable is the same with the cable used in LCC-HVDC case. For the sake of brevity, only a brief comparison is made between the obtained results in this case and the results extracted in the case of LCC-HVDC. The ratios of different resources in demand supply in both VSC and LCC link in RA strategy are shown in Fig. 13. The pool share in VSC technology is slightly less than LCC (maximum 7.64%). The other shares are almost the same compared to LCC technology. The ratios of different resources in demand supply in both VSC and LCC link in RS strategy are given in Fig. 14. In this case, the pool share in VSC technology is again less than LCC (maximum 5.37%). The other share ratios are almost the same compared to LCC technology.

- Comparing the LCC and VSC technologies shows that both of them give close results in terms of different resources shares for supplying the demand. However, (as can be seen in Fig. 15) LCC technology provides more robust solution compared to VSC technology. This means for a given ς_c the LCC gives a higher value of $\hat{\zeta}$ compared to VSC. So the decision maker is less worried about the uncertainty of wind generation to increase the total costs in risk averse strategy.
- In risk seeker approach, the LCC is superior compared to VSC technology. The provided solution by LCC requires less chance compared to VSC to happen. This means for the given solution of LCC, the decision maker is more probable to achieve the success (experience the less total

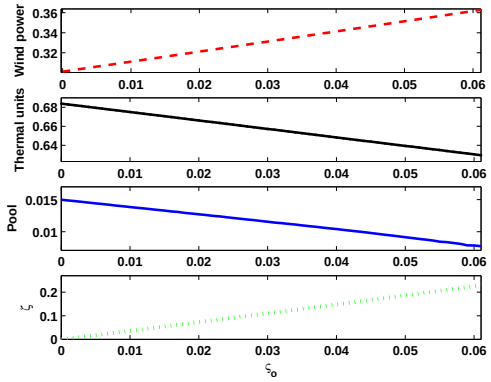

Fig. 9. Participation from different procurement options in RS strategy (LCC-HVDC)

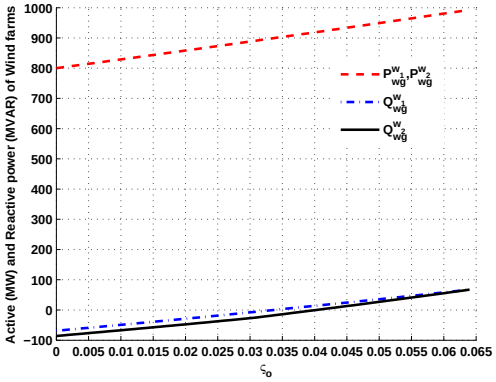

Fig. 11. Variations of active/reactive power of different wind farms vs ς_o in RS case (LCC-HVDC)

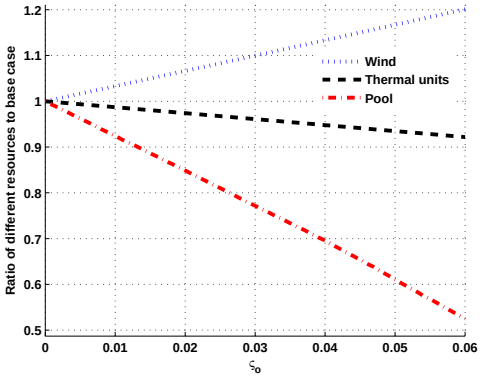

Fig. 10. Ratio of different resources to their corresponding base case values vs ς_o in RS strategy (LCC-HVDC)

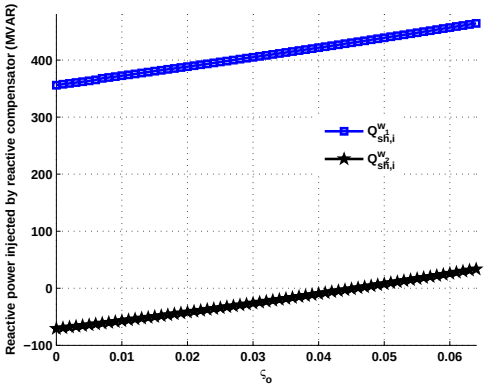

Fig. 12. Variation of reactive power injections vs ς_o at both sides of HVDC links in RS strategy (LCC-HVDC)

cost than the predicted value). This is demonstrated in Fig. 16, where for every given value of ς_o the radius of uncertainty is less in LCC than in VSC technology.

V. Conclusion

This paper presents a comprehensive OPF formulation which describes a power system with uncertain wind power injection through LCC-HVDC links. The objective is defined as maximizing the robustness of total costs against the intermittent wind power generation using Info-Gap decision theory. The proposed approach is tested on 118-bus IEEE system to demonstrate its applicability. The conclusions drawn from this work are listed as follows:

1) The opportunity of lower costs increases with the increase of HVDC-link reactive support, conversely robustness of the decision increases with lower reactive of HVDC-link.
2) The proposed IGDT strategy is exact and the obtained results are reliable for decision maker.
3) The computation burden of risk averse/seeker strategy is the same as base case (risk neutral). This means that the proposed technique is not computationally expensive compared to other uncertainty handling tools.
4) The proposed strategies are applicable even if no probability density function is available for wind power generation (severe uncertainty).
5) The power factor of each wind farm plays a key role in both risk averse and risk seeker strategies.
6) The interesting feature of the proposed model is that it can provide risk averse strategy to be immune against the wind power generation reduction. This reduction may have different technical reasons such as wind speed forecast error, non-optimal power tracking [15], equipment failures and etc. The authors would elaborate future work to quantify the impact of each technical reason individually.

References

[1] W. Lin, J. Wen, S. Cheng, and W.-J. Lee, "An investigation on the active-power variations of wind farms," *Industry Applications, IEEE Transactions on*, vol. 48, no. 3, pp. 1087–1094, May 2012.

[2] H. Ergun, D. Van Hertem, and R. Belmans, "Transmission system topology optimization for large-scale offshore wind integration," *Sustainable Energy, IEEE Transactions on*, vol. 3, no. 4, pp. 908–917, Oct 2012.

[3] J. Liang, T. Jing, O. Gomis-Bellmunt, J. Ekanayake, and N. Jenkins, "Operation and control of multiterminal hvdc transmission for offshore wind farms," *IEEE Transactions on Power Delivery*, vol. 26, no. 4, pp. 2596–2604, Oct 2011.

[4] P. Chen, P. Siano, Z. Chen, and B. Bak-Jensen, "Optimal allocation of power-electronic interfaced wind turbines using a genetic algorithm–monte carlo hybrid optimization method," in *Wind Power Systems*. Springer, 2010, pp. 1–23.

[5] A. Soroudi and T. Amraee, "Decision making under uncertainty in energy systems: State of the art," *Renewable and Sustainable Energy Reviews*, vol. 28, no. 0, pp. 376 – 384, 2013.

[6] C. Saunders, "Point estimate method addressing correlated wind power for probabilistic optimal power flow," *Power Systems, IEEE Transactions on*, vol. 29, no. 3, pp. 1045–1054, May 2014.

[7] A. Soroudi and A. Rabiee, "Optimal multi-area generation schedule considering renewable resources mix: a real-time approach," *Generation, Transmission Distribution, IET*, vol. 7, no. 9, pp. 1011–1026, Sept 2013.

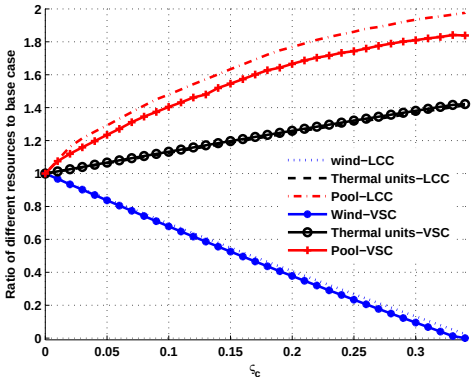

Fig. 13. Ratios of different resources in demand supply in both VSC and LCC link in RA strategy

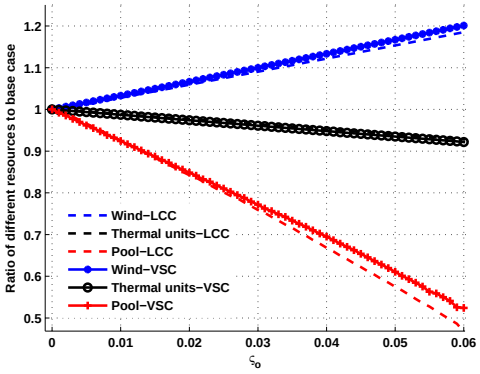

Fig. 14. Ratios of different resources in demand supply in both VSC and LCC link in RS strategy

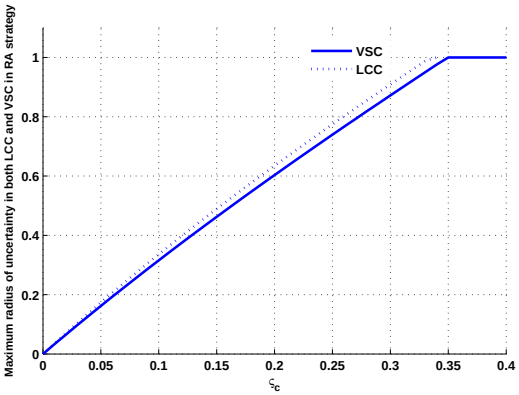

Fig. 15. Maximum radius of uncertainty ($\hat{\zeta}$) compared in VSC and LCC HVDC links for Risk averse strategy (RA)

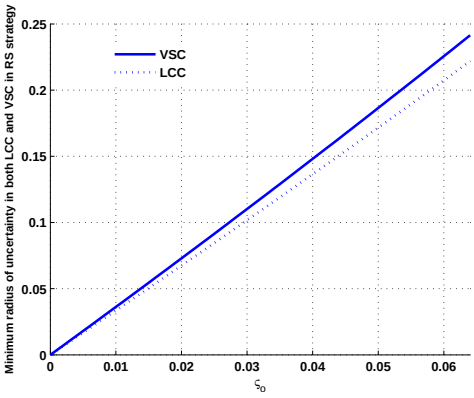

Fig. 16. Minimum radius of uncertainty ($\check{\zeta}$) compared in VSC and LCC HVDC links for Risk seeker strategy (RS)

[8] A. Rabiee, A. Soroudi, B. Mohammadi-ivatloo, and M. Parniani, "Corrective voltage control scheme considering demand response and stochastic wind power," *Power Systems, IEEE Transactions on*, vol. 29, no. 6, pp. 2965–2973, Nov 2014.

[9] A. Soroudi, "Possibilistic-scenario model for dg impact assessment on distribution networks in an uncertain environment," *IEEE Transactions on Power Systems*, vol. 27, no. 3, pp. 1283–1293, Aug 2012.

[10] R. Jabr, "Adjustable robust opf with renewable energy sources," *Power Systems, IEEE Transactions on*, vol. 28, no. 4, pp. 4742–4751, Nov 2013.

[11] A. Soroudi, "Robust optimization based self scheduling of hydro-thermal genco in smart grids," *Energy*, vol. 61, no. 0, pp. 262 – 271, 2013.

[12] L. Wang and M. N. Thi, "Stability enhancement of a pmsg-based offshore wind farm fed to a multi-machine system through an lcc-hvdc link," *Power Systems, IEEE Transactions on*, vol. 28, no. 3, pp. 3327–3334, Aug 2013.

[13] C. Yuan, X. Yang, D. Yao, and C. Yue, "Review on hybrid hvdc technology for integration of offshore wind power plant," in *Wind integration workshop, London , UK*, September 2013, pp. 1–5.

[14] R. Li, S. Bozhko, and G. Asher, "Frequency control design for offshore wind farm grid with lcc-hvdc link connection," *Power Electronics, IEEE Transactions on*, vol. 23, no. 3, pp. 1085–1092, May 2008.

[15] S. Bernal-Perez, S. Ano-Villalba, R. Blasco-Gimenez, and J. Rodriguez-D'Derlee, "Efficiency and fault ride-through performance of a diode-rectifier- and vsc-inverter-based hvdc link for offshore wind farms," *Industrial Electronics, IEEE Transactions on*, vol. 60, no. 6, pp. 2401–2409, June 2013.

[16] B. Andersen, "Vsc transmission tutorial," in *CIGRE Study Commitee B4 Meeting, Bangalore*, 2005.

[17] A. Elserougi, A. Massoud, A. Abdel-Khalik, and S. Ahmed, "Bidirectional buck-boost inverter-based hvdc transmission system with ac-side contribution blocking capability during dc-side faults," *Power Delivery, IEEE Transactions on*, vol. 29, no. 3, pp. 1249–1261, June 2014.

[18] S. M. Muyeen, R. Takahashi, and J. Tamura, "Operation and control of hvdc-connected offshore wind farm," *Sustainable Energy, IEEE Transactions on*, vol. 1, no. 1, pp. 30–37, April 2010.

[19] L. Wang and M. S. N. Thi, "Comparative stability analysis of offshore wind and marine-current farms feeding into a power grid using hvdc links and hvac line," *Power Delivery, IEEE Transactions on*, vol. 28, no. 4, pp. 2162–2171, Oct 2013.

[20] C.-J. Chou, Y.-K. Wu, G.-Y. Han, and C.-Y. Lee, "Comparative evaluation of the hvdc and hvac links integrated in a large offshore wind farm;an actual case study in taiwan," *Industry Applications, IEEE Transactions on*, vol. 48, no. 5, pp. 1639–1648, Sept 2012.

[21] K. Burman, D. Olis, V. Gevorgian, A. Warren, R. Butt, P. Lilienthal, and J. Glassmire, "Integrating renewable energy into the transmission and distribution system of the us virgin islands," National Renewable Energy Laboratory (NREL), Golden, CO., Tech. Rep., 2011.

[22] S. Chaudhary, R. Teodorescu, P. Rodriguez, P. Kjaer, and A. Gole, "Negative sequence current control in wind power plants with vsc-hvdc connection," *Sustainable Energy, IEEE Transactions on*, vol. 3, no. 3, pp. 535–544, July 2012.

[23] A. Egea-Alvarez, F. Bianchi, A. Junyent-Ferre, G. Gross, and O. Gomis-Bellmunt, "Voltage control of multiterminal vsc-hvdc transmission systems for offshore wind power plants: Design and implementation in a scaled platform," *Industrial Electronics, IEEE Transactions on*, vol. 60, no. 6, pp. 2381–2391, June 2013.

[24] L. Xu, L. Yao, and C. Sasse, "Grid integration of large dfig-based wind farms using vsc transmission," *Power Systems, IEEE Transactions on*, vol. 22, no. 3, pp. 976–984, Aug 2007.

[25] R. Torres-Olguin, M. Molinas, and T. Undeland, "Offshore wind farm grid integration by vsc technology with lcc-based hvdc transmission," *Sustainable Energy, IEEE Transactions on*, vol. 3, no. 4, pp. 899–907, Oct 2012.

[26] W. Feng, A. L. Tuan, L. Tjernberg, A. Mannikoff, and A. Bergman, "A new approach for benefit evaluation of multiterminal vsc x2013;hvdc using a proposed mixed ac/dc optimal power flow," *IEEE Transactions on Power Delivery*, vol. 29, no. 1, pp. 432–443, Feb 2014.

[27] L. Shi, C. Wang, L. Yao, Y. Ni, and M. Bazargan, "Optimal power flow solution incorporating wind power," *Systems Journal, IEEE*, vol. 6, no. 2, pp. 233–241, 2012.

[28] M. Montilla-DJesus, D. Santos-Martin, S. Arnaltes, and E. Castronuovo,

"Optimal reactive power allocation in an offshore wind farms with lcc-hvdc link connection," *Renewable Energy*, 2011.
[29] R. Jabr and B. Pal, "Intermittent wind generation in optimal power flow dispatching," *Generation, Transmission & Distribution, IET*, vol. 3, no. 1, pp. 66–74, 2009.
[30] P. Yu and B. Venkatesh, "A practical real-time opf method using new triangular approximate model of wind electric generators," *IEEE Transactions on Power Systems,*, vol. to appear, 2012.
[31] A. Tapia, G. Tapia, and J. Ostolaza, "Reactive power control of wind farms for voltage control applications," *Renewable Energy*, vol. 29, no. 3, pp. 377 – 392, 2004.
[32] M. A. Tajeddini, A. Rahimi-Kian, and A. Soroudi, "Risk averse optimal operation of a virtual power plant using two stage stochastic programming," *Energy*, vol. 73, no. 0, pp. 958 – 967, 2014.
[33] D. Santos-Martin, S. Arnaltes, and J. R. Amenedo, "Reactive power capability of doubly fed asynchronous generators," *Electric Power Systems Research*, vol. 78, no. 11, pp. 1837 – 1840, 2008.
[34] M. Montilla-DJesus, D. Santos-Martin, S. Arnaltes, and E. Castronuovo, "Optimal operation of offshore wind farms with line-commutated hvdc link connection," *Energy Conversion, IEEE Transactions on*, vol. 25, no. 2, pp. 504 –513, june 2010.
[35] A. Pizano-Martinez, C. R. Fuerte-Esquivel, H. Ambriz-Perez, and E. Acha, "Modeling of vsc-based hvdc systems for a newton-raphson opf algorithm," *Power Systems, IEEE Transactions on*, vol. 22, no. 4, pp. 1794–1803, 2007.
[36] E. Acha, C. R. Fuerte-Esquivel, H. Ambriz-Perez, and C. Angeles-Camacho, *FACTS: modelling and simulation in power networks*. John Wiley & Sons, 2004.
[37] A. Soroudi and M. Ehsan, "Igdt based robust decision making tool for dnos in load procurement under severe uncertainty," *Smart Grid, IEEE Transactions on*, vol. 4, no. 2, pp. 886–895, June 2013.
[38] Https://sites.google.com/site/alirezasoroudi/DATAIEEE118.xlsx.
[39] R. Zimmerman, C. Murillo-Sánchez, and R. Thomas, "Matpower: Steady-state operations, planning, and analysis tools for power systems research and education," *Power Systems, IEEE Transactions on*, vol. 26, no. 1, pp. 12–19, 2011.
[40] 'GAMS', "A user guide," New York, Tech. Rep., 2008.
[41] A. Rabiee and A. Soroudi, "Stochastic multiperiod opf model of power systems with hvdc-connected intermittent wind power generation," *IEEE Transactions on Power Delivery*, vol. 29, no. 1, pp. 336–344, Feb 2014.

Abbas Rabiee (M14) Received the B.Sc. degree in electrical engineering from Iran University of Science and Technology (IUST), Tehran, in 2006, and the M.Sc. and Ph.D. degrees in electrical power engineering from Sharif University of Technology (SUT), Tehran, Iran, in 2008 and 2013, respectively. Currently, he is an Assistant Professor at the Department of Electrical Engineering, Faculty of Engineering, University of Zanjan, Zanjan, Iran. His research interests include power system operation and security, renewable energies, and the application of optimization techniques in power system operation.

Alireza Soroudi (M14) Received the B.Sc. and M.Sc. degrees from Sharif University of Technology, Tehran, Iran, in 2002 and 2004, respectively, both in electrical engineering. and Ph.D. degree from Grenoble Institute of Technology (Grenoble-INP), Grenoble, France, in 2011. He is the winner of the ENRE Young Researcher Prize at the INFORMS 2013. He is currently a senior researcher with the School of Electrical, Electronic, and Mechanical Engineering, University College Dublin with research interests in uncertainty modelling and optimization techniques applied to Smart grids, power system planning and operation.

Andrew Keane (S04M07) received the B.E. and Ph.D. degrees in electrical engineering from University College Dublin, Dublin, Ireland, in 2003 and 2007, respectively. He is currently a lecturer with the School of Electrical, Electronic, and Mechanical Engineering, University College Dublin with research interests in power systems planning and operation, distributed energy resources, and distribution networks.